On the nonlinear behavior of Boussinesq type models : amplitude-velocity vs amplitude-flux forms

A.G. Filippini*, S. Bellec*,+, M. Colin*,+, and M. Ricchiuto*

* Inria Bordeaux - Sud-Ouest,
200 Avenue de la Vieille Tour, 33405 Talence cedex - France

+ Institut de Mathématiques de Bordeaux,
351 cours de la Libération, 33405 Talence cedex - France

1 Introduction

The modeling of wave transformation in the near shore region requires a physically correct description of both dispersive and nonlinear effects. The use of asymptotic depth averaged Boussinesq Type (BT) models for this task is quite common [6]. These models have to be used with much care. Quite often, weakly-nonlinear variants of these models, such as those proposed in [1, 4, 15, 16, 18], are used outside of their range of applicability, e.g. when reaching breaking conditions. In these cases fully-nonlinear models should be used instead [9]. Moreover, to actually include the energy dissipation effects associated to wave breaking, either ad-hoc viscosity terms are included, or a coupling with the Shallow Water equations is introduced [22, 21, 6, 11]. Despite of the fact that they are theoretically well adapted only for small amplitude waves, in practice these models provide accurate results also when used outside they domain of validity [20, 6, 11].

The key to this success is actually the use of a properly designed wave breaking model, which includes a breaking detection criterion, and a dissipation mechanism. The challenge for a correct capturing of these fronts, is the understanding of the genuinely nonlinear physics underlying breaking, as well as the behavior of the underlying dispersive wave propagation model, and in particular the wave shoaling when approaching the nonlinear regime. Accounting for genuinely nonlinear effects is thus a research topic of high priority [6]. While the linear properties of the models can be thoroughly studied analytically [8], in the nonlinear case some properties, such as e.g. the shoaling behavior, must be studied numerically.

There exist several types of weakly nonlinear BT models. These all provide different approximations of the nonlinear wave (or Euler) equations. The design properties of these models are often the linear dispersion relation and shoaling coefficients which should be as close as possible to those of the linear wave theory for in the range of wave numbers relevant for the applications sought. Given a linear dispersion relation and linear shoaling coefficient, it is known that two nonlinear set of Partial Differential Equations (PDEs) can be formulated,

both degenerating to the same linearized system. Denoting by a the wave amplitude, d the mean water level, and λ the wavelength, these two models are alternate forms within the same asymptotics in terms of the nonlinearity $\varepsilon = a/d$ and dispersion $\sigma = d/\lambda$ parameters. The main difference is in the nature of the higher order derivatives, which can either be applied to the velocity u, or to the flux $q = hu$, h denoting the depth. These formulations are referred here to as *amplitude-velocity*, and *amplitude-volume flux* forms. Examples of such couples for some dispersion relations are given for example in [8].

To gain better understanding in the properties of weakly nonlinear BT models, this paper presents a thorough analytical and numerical characterization of their nonlinear behavior. For a given couple linear dispersion relation-linear shoaling parameter, we start by recalling how to construct, within the same asymptotic accuracy, two nonlinear set of PDEs : one in amplitude-velocity form, the other in amplitude-volume flux form. The theory is applied to four linear relations corresponding to the models of Peregrine [18], and to the enhanced models of Beji and Nadaoka [4], Madsen and Sørensen [15], and Nwogu [16]. For each of these models, we show the corresponding alternate formulation. We will show that the amplitude-volume flux form of the Peregrine system leads to the model used by Abbott in [1], that the amplitude-volume flux form of the Beji and Nadaoka model actually correspond to a slight modification of the Madsen and Sørensen model, and vice versa that the amplitude-velocity form of the latter can be obtained by a small modification of the model of [4]. Finally, for the equations of Nwogu, we derive a new BT system which is the corresponding amplitude-volume flux form. We then study these models, and the main result of the paper can be summarized as follows : while in the linearized case four types of behaviors are observed, corresponding to the given four linear relations, when approaching the nonlinear regime, only two type of behaviors are observed, which are practically independent on the linear dispersion relations and shoaling parameters, and only depend on whether the model is in amplitude-velocity or amplitude-volume flux form. This observation is confirmed by both theoretical arguments, and numerical results.

The present study gives important insight in the behavior of BT models, especially in view of the applications of breaking detection criteria. In particular, our result shows that these criteria must not only take into account the type of breaking expected in the flow, but also the underlying form of the propagation model. For simplicity, we only consider here models well suited for the near shore range (reduced wave numers $kd \leq \pi$), however very similar arguments can be used to study deep water variants [14].

The structure of the paper is the following. In section §2. we present the derivation of weakly nonlinear Boussinesq equations, and we discuss the construction of models in amplitude-velocity, and amplitude-flux forms for different particular cases. Section §3 presents the theoretical analysis of the systems of PDEs obtained, and in particular the analysis of the propagation of higher order harmonics, which gives an indication of the non-linear behavior of the models. Finally, numerical tests in both the linear and nonlinear regime are discussed in section §4. The paper is ended by conclusive remarks and by an overview of future works.

2 Weakly nonlinear Boussinesq type models

We review a certain number of weakly nonlinear Boussinesq type (BT) models. We recall that these models are obtained as depth averaged asymptotic approximations of the incompressible Euler equations. In particular, if a denotes a reference wave amplitude, d_0 a reference water depth, and λ a typical wavelength, we consider the nonlinearity parameter ϵ and the dispersion parameter σ defined by

$$\epsilon = \frac{a}{d_0}\,, \quad \sigma = \frac{d_0}{\lambda}\,.$$

Weakly dispersive BT models are obtained under the small amplitude hypothesis $\epsilon = \mathcal{O}(\sigma^2)$, as asymptotic approximations of the order $\mathcal{O}(\epsilon\sigma^2,\, \sigma^4)$. We refer to [8, 12] for details concerning the basic derivation of the models. Our objective is to recall some of the models most commonly encountered in literature, and to discuss the construction of amplitude-velocity and amplitude-flux forms having the same linearized behavior.

In the following sections we use the notation $d(x)$ for the variable mean/still water level, η for the wave amplitude w.r.t. a reference zero level, and $h = \eta + d$ for the depth (cf. figure 1),

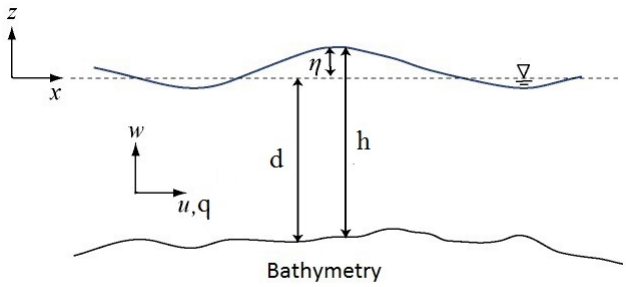

Figure 1: Sketch of the free surface flow problem, main parameters description.

2.1 Models of Peregrine and Abbott

The most common BT model is the one introduced by Peregrine in [18]:

$$\begin{cases} \eta_t + \left[(d+\eta)u\right]_x = 0 \\ u_t + uu_x + g\eta_x - \left(\dfrac{d}{2}[du]_{xxt} - \dfrac{d^2}{6}u_{xxt}\right) = 0 \end{cases}. \tag{1}$$

Here u denotes the depth-average velocity. If we multiplying the first equation of (1) by u, the second one by h and summing up the resulting expressions, we can rewrite the Peregrine equations in terms of the conservative variables (h, q), with $q = hu$ the volume flux. Denoting the Non-Linear Shallow Water (NLSW) flux by

$$F^{SW} = \frac{q^2}{h} + g\frac{h^2}{2}\,, \tag{2}$$

we obtain:

$$\begin{cases} h_t + q_x = 0 \\ q_t + F_x^{SW} - ghd_x - hP_t(u) = 0 \end{cases} \tag{3}$$

System (3) allows to underline the structure of the Peregrine model, which is obtained by adding to the NLSW equations a term given by the depth times the time derivative of an elliptic linear differential operator applied to the depth averaged velocity u. This elliptic operator, denoted by $P(\cdot)$ in (3), is defined by :

$$P(\cdot) = \frac{d}{2}[(\cdot)d]_{xx} - \frac{d^2}{6}(\cdot)_{xx}\,. \tag{4}$$

To proceed further, we consider now the non-dimensional form of (1). To this end, we recall that the reference depth, amplitude, and wavelength are denoted by d_0, a, and λ respectively. Introducing a typical horizontal length scale L, we then introduce the set of non-dimensional variables :

$$\tilde{x} = \frac{x}{L},\quad \tilde{t} = \frac{\sqrt{gd_0}}{L}t,\quad \tilde{\eta} = \frac{\eta}{a},\quad \tilde{d} = \frac{d}{d_0},\quad \tilde{u} = \frac{d_0}{a\sqrt{gd_0}}u\,.$$

With this notation, one can easily show that (1) is equivalent to :

$$\begin{cases} \tilde{\eta}_{\tilde{t}} + \left[(\tilde{d}+\varepsilon\tilde{\eta})\tilde{u}\right]_{\tilde{x}} = 0 \\ \tilde{u}_{\tilde{t}} + \varepsilon\tilde{u}\tilde{u}_{\tilde{x}} + \tilde{\eta}_{\tilde{x}} - \sigma^2\left(\frac{\tilde{d}}{2}[\tilde{d}\tilde{u}]_{\tilde{x}\tilde{x}} - \frac{\tilde{d}^2}{6}\tilde{u}_{\tilde{x}\tilde{x}}\right)_{\tilde{t}} = 0 \end{cases}. \tag{5}$$

We recall that the truncation w.r.t. the Euler equations, which should appear on the right hand side, is of order $\mathscr{O}(\varepsilon\sigma^2, \sigma^4)$. We now repeat the same algebraic steps done previously : we multiply the first equation by $\varepsilon\tilde{u}$, the second one by $\tilde{h} = \tilde{d} + \varepsilon\tilde{\eta}$, and we add the expressions thus obtained, resulting in

$$\left[(\tilde{d}+\varepsilon\tilde{\eta})\tilde{u}\right]_{\tilde{t}} + \left[\epsilon\tilde{u}(\tilde{d}+\varepsilon\tilde{\eta})\tilde{u}\right]_{\tilde{x}} + \epsilon\tilde{\eta}\tilde{\eta}_{\tilde{x}} + \tilde{d}\tilde{\eta}_{\tilde{x}} - (\tilde{d}+\varepsilon\tilde{\eta})\sigma^2\left(\frac{\tilde{d}}{2}[\tilde{d}\tilde{u}]_{\tilde{x}\tilde{x}} - \frac{\tilde{d}^2}{6}\tilde{u}_{\tilde{x}\tilde{x}}\right)_{\tilde{t}} = 0\,.$$

Since $\tilde{d}\tilde{u} = \tilde{q} + \mathscr{O}(\varepsilon)$, we deduce that:

$$(\tilde{d}+\varepsilon\tilde{\eta})\sigma^2\left(\frac{\tilde{d}}{2}[\tilde{d}\tilde{u}]_{\tilde{x}\tilde{x}} - \frac{\tilde{d}^2}{6}\tilde{u}_{\tilde{x}\tilde{x}}\right) = \sigma^2\left(\frac{\tilde{d}^2}{2}\tilde{q}_{\tilde{x}\tilde{x}} - \frac{\tilde{d}^3}{6}(\frac{\tilde{q}}{\tilde{d}})_{\tilde{x}\tilde{x}}\right) + \mathscr{O}(\varepsilon\sigma^2, \sigma^4)\,. \tag{6}$$

As a consequence, an asymptotically equivalent system is obtained by replacing the second equation in (5) by

$$\left[(\tilde{d}+\varepsilon\tilde{\eta})\tilde{u}\right]_{\tilde{t}} + \left[\epsilon\tilde{u}(\tilde{d}+\varepsilon\tilde{\eta})\tilde{u}\right]_{\tilde{x}} + \epsilon\tilde{\eta}\tilde{\eta}_{\tilde{x}} + \tilde{d}\tilde{\eta}_{\tilde{x}} - \sigma^2\left(\frac{\tilde{d}^2}{2}\tilde{q}_{\tilde{x}\tilde{x}} - \frac{\tilde{d}^3}{6}(\frac{\tilde{q}}{\tilde{d}})_{\tilde{x}\tilde{x}}\right)_{\tilde{t}} = 0\,. \tag{7}$$

Coming back to dimensional quantities, we obtain the following BT model presented by Abbott in [1] :

$$\begin{cases} h_t + q_x = 0 \\ Q_t(q) + F_x^{SW} - ghd_x = 0 \end{cases} \tag{8}$$

In the linearized case, the models of Peregrine and of Abbott are identical, so the two systems have the same linear dispersive and linear shoaling characteristics. In the nonlinear case, the two systems are both approximations of the Euler equations of order $\mathscr{O}(\varepsilon\sigma^2, \sigma^4)$, however they do differ as the dispersive terms are expressed in terms of the derivatives of u in the Peregrine one and in terms of the derivatives of q in (8). In the latter, we see once more the appearance of the time derivative of a linear elliptic operator, denoted by $Q(\cdot)$ and defined by :

$$Q(\cdot) = (\cdot) - d\left(\frac{d}{2}(\cdot)_{xx} - \frac{d^2}{6}\left[\frac{(\cdot)}{d}\right]_{xx}\right) \tag{9}$$

Compared to (3), system (8) has a more compact and seemingly conservative structure, as it does not involve any additional non-conservative product w.r.t the NLSW equations.

The limited accuracy systems (1) and (8), e.g. in terms of linear dispersion relations, has pushed the development of the so-called enhanced models. These are improved approximations which, while still remaining of order $\mathscr{O}(\varepsilon\sigma^2, \sigma^4)$ w.r.t the Euler equations, provide substantially improved approximations of the linearized dispersion relations and shoaling coefficients of the original three dimensional equations. These models are considered in the following sections.

2.2 Beji-Nadaoka and BNA models

Following [4], an improved system can be obtained as follows : starting from the non-dimensional system of Peregrine (5), we add and subtract the term $\sigma^2\alpha_B P(\tilde{u}_{\tilde{t}})$; we then use the fact that in the non-dimensional form $\tilde{u}_{\tilde{t}} + \tilde{\eta}_{\tilde{x}} = \mathscr{O}(\varepsilon, \sigma^2)$ to replace $+\sigma^2\alpha_B P(\tilde{u}_{\tilde{t}})$ by $-\sigma^2\alpha_B P(\tilde{\eta}_{\tilde{x}})$ plus orders of $\mathscr{O}(\varepsilon\sigma^2, \sigma^4)$ which can be neglected. The final result is the enhanced system proposed by Beji and Nadaoka [4] (model BN), in dimensional variables reading :

$$\begin{cases} \eta_t + q_x = 0 \\ u_t + uu_x + g\eta_x - (1+\alpha_B)P_t(u) - g\alpha_B P(\eta_x) = 0 \end{cases} \tag{10}$$

with $P(\cdot)$ the elliptic operator (4). The model of Beji and Nadaoka can be also written in terms of the conservative variables (h, q) as :

$$\begin{cases} h_t + q_x = 0 \\ q_t + F_x^{SW} - ghd_x - (1+\alpha_B)hP_t(u) - gh\alpha_B P(\eta_x) = 0 \end{cases} \tag{11}$$

The additional free parameter α_B allows to improve the dispersion relation of the system w.r.t. the one of Peregrine's model.

System (11) is in amplitude-velocity form, as the dispersive terms involve derivatives of the velocity and not of the flux q. We can derive an asymptotically equivalent system in amplitude-flux form proceeding exactly as done for the Peregrine equations in non-dimensional form (details are omitted for brevity). The final result is the *Beji-Nadaoka-Abbott* model (BNA) reading :

$$\begin{cases} h_t + q_x = 0 \\ \check{Q}_t(q) + F_x^{SW} - ghd_x - gd\alpha_B P(\eta_x) = 0 \end{cases} \tag{12}$$

where the operator $\check{Q}(\cdot)$ is very close to $Q(\cdot)$ in (9), except for the presence of the tuning parameter α_B :

$$\check{Q}(\cdot) = (\cdot) - (1+\alpha_B)d\left(\frac{d}{2}(\cdot)_{xx} - \frac{d^2}{6}\left[\frac{(\cdot)}{d}\right]_{xx}\right) \tag{13}$$

While for $\alpha_B = 0$ system (11) reduces to the model of Peregrine, model (12) reduces in this limit to the equations of Abbott. When $\alpha_B \neq 0$ the BNA model has a less compact form, compared to (8), due to the presence of the additional term $-g\alpha_B dP(\eta_x)$.

2.3 Madsen-Sørensen and MSP models

The enhanced model proposed by Madsen and Sørensen in [15] is obtained with a procedure very similar to the one discussed in the previous paragraph : starting from the non-dimensional form of the second equation in Abbott's model (7), we add and subtract the quantity $\sigma^2\beta\tilde{q}_{\tilde{x}\tilde{x}\tilde{t}}$; we then use the facts that $\tilde{q}_{\tilde{t}} + \tilde{h}\tilde{\eta}_{\tilde{x}} = \mathscr{O}(\varepsilon, \sigma^2)$ and that $\tilde{h} = \tilde{d} + \mathscr{O}(\varepsilon)$ to replace $+\sigma^2\alpha_M\tilde{q}_{\tilde{x}\tilde{x}\tilde{t}}$ with $-\sigma^2\beta(\tilde{d}\tilde{\eta}_{\tilde{x}})_{\tilde{x}\tilde{x}}$. The system analyzed in [15] is finally obtained by neglecting all terms of order $\mathscr{O}(\varepsilon\sigma^2, \sigma^4)$, and in the mild slope hypothesis by neglecting terms containing d_x^2 and d_{xx}. The resulting equations read :

$$\begin{cases} h_t + q_x = 0 \\ \bar{Q}_t(q) + F_x^{SW} - ghd_x - g\beta d\hat{P}(\eta_x) = 0 \end{cases}, \tag{14}$$

where $\hat{P}(\cdot)$ and $\bar{Q}(\cdot)$ are defined by :

$$\hat{P}(\cdot) = d^2(\cdot)_{xx} + 2dd_x(\cdot)_x\,, \tag{15}$$

and

$$\bar{Q}(\cdot) = (\cdot) - \left(\frac{1}{3} + \beta\right)d^2(\cdot)_{xx} - \frac{d}{3}d_x(\cdot)_x\,, \tag{16}$$

The system reduces exactly to the one of Abbott for the choice of $\beta = 0$, but it has a more complex structure due to the term $g\beta d\hat{P}(\eta_x)$. The free parameter β, however, allows to substantially improve the linear dispersion and shoaling properties w.r.t. (8).

The model is clearly in amplitude-flux form, and an asymptotically equivalent in wave amplitude velocity form can be obtained by manipulations of the non-dimensional form of the equations very similar to those done for the other models (details omitted for brevity). The final form of the model in the mild slope hypothesis is

$$\begin{cases} h_t + q_x = 0 \\ q_t + F_x^{SW} - ghd_x + h\bar{P}_t(u) - \beta gh\hat{P}(\eta_x) = 0 \end{cases}, \tag{17}$$

with

$$\bar{P}(\cdot) = -\left(\frac{1}{3} + \beta\right) d^2(\cdot)_{xx} - (1+2\beta)dd_x(\cdot)_x\,, \tag{18}$$

In this case the limit $\beta = 0$ gives back the model of Peregrine (3), however (17) has substantially improved linear characteristics. In the following we will refer to this model as to the *Madsen-Sørensen-Peregrine* system (MSP).

Note that simple manipulations show that in the case of $d = const$, the BN and the MSP systems as well as the BNA and the MS systems collapse onto one another provided that $\beta = \alpha_B/3$. All these models indeed share the same linear dispersion relation. For non-constant bathymetries, these models define two families of linear shoaling parameters, as we will see in section 3.1.

2.4 Nwogu and NA models

The study of enhanced Boussinesq equations would not be complete without taking into account the model of extended model of Nwogu [16]. This model is obtained by enhancing the system of Peregrine by replacing the depth averaged velocity by the velocity at an arbitrary elevation z_θ. For simplicity, in the following developments we still denote by u the quantity $u(t, x, z = z_\theta)$, but it should be clear that the physical meaning of this quantity is different from the depth averaged horizontal speed present in all the previous models. Setting $z_\theta = \theta d$, for some $\theta \in (-1, 0)$, the model of Nwogu can be written as [16] :

$$\begin{cases} \eta_t + \left[q + dP^b(u)\right]_x = 0 \\ u_t + uu_x + g\eta_x + P_t^a(u) = 0 \end{cases} \tag{19}$$

This model has a more complex structure, with additional operators appearing in both equations. In particular, the operators $P^a(\cdot)$ and $P^b(\cdot)$ are linear elliptic operators with identical structure to $P(\cdot)$ appearing in the Peregrine system (cf. equation (4)), but with different coefficients:

$$P^a(\cdot) = a_1\frac{d^2}{6}(\cdot)_{xx} - a_2\frac{d}{2}[(\cdot)d]_{xx}\,, \tag{20}$$

$$P^b(\cdot) = b_1\frac{d^2}{6}(\cdot)_{xx} - b_2\frac{d}{2}[(\cdot)d]_{xx}\,, \tag{21}$$

The values of such coefficients are expressed as function of the tuning parameter θ and read :

$$a_1 = 3\theta^2; \quad a_2 = -2\theta; \quad b_1 = 3\theta^2 - 1; \quad b_2 = -2\theta - 1\,.$$

The equations of Peregrine are recovered for the choice $a_1 = a_2 = 1,\ b_1 = b_2 = 0$. Note that it is not possible to find a unique value $\theta \in (-1, 0)$, such that this condition is verified. With simple manipulations, we can recast model (19) in terms of time evolution of the flux q as :

$$\begin{cases} h_t + \left[q + dP^b(u)\right]_x = 0 \\ q_t + F_x^{SW} - ghd_x + hP_t^a(u) + u\left[dP^b(u)\right]_x = 0 \end{cases} \tag{22}$$

Last equations show that, among the amplitude-velocity enhanced models, the model of Nwogu is the one with the most complex structure when written for the couple (η, q)

We now aim to find an asymptotically equivalent system in amplitude-flux form which degenerates to the same linearized equations as the model of Nwogu. Retracing steps already made in the previous subsections, we first consider the non-dimensional form of (19) :

$$\begin{cases} \tilde{\eta}_{\tilde{t}} + \left[(\tilde{d} + \varepsilon\tilde{\eta})\tilde{u} + \sigma^2\left(b_1\dfrac{\tilde{d}^2}{6}\tilde{u}_{\tilde{x}\tilde{x}} - b_2\dfrac{\tilde{d}}{2}[\tilde{u}\tilde{d}]_{\tilde{x}\tilde{x}}\right)\right]_{\tilde{x}} = 0 \\ \tilde{u}_{\tilde{t}} + \varepsilon\tilde{u}\tilde{u}_{\tilde{x}} + g\tilde{\eta}_{\tilde{x}} + \sigma^2\left(a_1\dfrac{\tilde{d}^2}{6}\tilde{u}_{\tilde{x}\tilde{x}} - a_2\dfrac{\tilde{d}}{2}[\tilde{u}\tilde{d}]_{\tilde{x}\tilde{x}}\right)_{\tilde{t}} = 0 \end{cases} \tag{23}$$

We multiply the first equation by $\varepsilon\tilde{u}$, and the second by $(\tilde{d} + \varepsilon\tilde{\eta})$, we sum the expressions obtained, and once more invoke the relations

$$(\tilde{d}+\varepsilon\tilde{\eta})\sigma^2\left(a_1\frac{\tilde{d}^2}{6}\tilde{u}_{\tilde{x}\tilde{x}} - a_2\frac{\tilde{d}}{2}[\tilde{d}\tilde{u}]_{\tilde{x}\tilde{x}}\right) = \sigma^2\left(a_1\frac{\tilde{d}^3}{6}(\frac{\tilde{q}}{\tilde{d}})_{\tilde{x}\tilde{x}} - a_2\frac{\tilde{d}^2}{2}\tilde{q}_{\tilde{x}\tilde{x}}\right) + \mathscr{O}(\varepsilon\sigma^2, \sigma^4) \tag{24}$$

and

$$\sigma^2\tilde{d}\left(b_1\frac{\tilde{d}^2}{6}\tilde{u}_{\tilde{x}\tilde{x}} - b_2\frac{\tilde{d}}{2}[\tilde{d}\tilde{u}]_{\tilde{x}\tilde{x}}\right) = \sigma^2\tilde{d}\left(b_1\frac{\tilde{d}^2}{6}(\frac{\tilde{q}}{\tilde{d}})_{\tilde{x}\tilde{x}} - b_2\frac{\tilde{d}}{2}\tilde{q}_{\tilde{x}\tilde{x}}\right) + \mathscr{O}(\varepsilon\sigma^2, \sigma^4) \tag{25}$$

to modify the linear dispersive terms. Neglecting the terms of order $\mathscr{O}(\varepsilon\sigma^2, \sigma^4)$, and coming back to the physical variables, we finally obtain the enhanced Boussinesq model :

$$\begin{cases} h_t + Q_x^b(q) = 0 \\ Q_t^a(q) + F_x^{SW} - ghd_x = 0 \end{cases} \tag{26}$$

where the operators $Q^a(\cdot)$ and $Q^b(\cdot)$ are defined by

$$Q^a(\cdot) = (\cdot) + d\left(a_1\frac{d^2}{6}\left[\frac{(\cdot)}{d}\right]_{xx} - a_2\frac{d}{2}(\cdot)_{xx}\right) \tag{27}$$

$$Q^b(\cdot) = (\cdot) + d\left(b_1 \frac{d^2}{6}\left[\frac{(\cdot)}{d}\right]_{xx} - b_2 \frac{d}{2}(\cdot)_{xx}\right) \tag{28}$$

The system obtained has a similar compact structure as (8), but it has the exact same linear characteristics of the equations of Nwogu. In this case, for $a_1 = a_2 = 1,\ b_1 = b_2 = 0$ we recover the model of Abbott. For this reason in the following we refer to these equations as the *Nwogu-Abbott* model (NA).

2.5 Summary

In this section we have considered the most popular BT models of the literature. We have shown that for each model, *viz* for a given pair of linear dispersion relation-linear shoaling coefficient, we can derive asymptotically equivalent amplitude-velocity and amplitude-flux forms. Some examples of these couples can be already found in [8]. We have given a thorough list of these couples, including a new form of Nwogu's model with a compact PDE structure similar to those of the equations of Abbott.

We summarize here the models which will be studied in the rest of the paper listing them couples having the same linearized system :

- Models of Peregrine (3) (amplitude-velocity) and of Abbott (8) (amplitude-flux) ;
- Model of Beji and Nadaoka (11) (amplitude-velocity) and BNA model (12) (amplitude-flux) ;
- Model of Madsen-Sørensen (14) (amplitude-flux) and MSP model (17) (amplitude-velocity) ;
- Model of Nwogu (19) (amplitude-velocity) and NA model (26) (amplitude-flux) .

The objective of the following sections is to study the properties of these systems. First, we will consider the aspect of wave propagation, in both the linear and nonlinear case. Then we will provide an analytical and numerical study of the linear and nonlinear shoaling characteristics of these models.

3 Theoretical analysis of the models

This section is devoted to the analysis of the theoretical properties of the models. In the linear case, the eight systems of PDEs introduced in section §2 reduce by construction to four families of linearized models. On constant bathymetries, the models of Beji and Nadaoka and of Madsen and Sørensen also degenerate to the same system of PDEs. In this case, we will briefly recall the linear dispersion analysis, and then discuss the behavior of second order harmonics. The analysis of the higher order harmonics will show that the nonlinear form of the system has a dramatic effect on the amplitudes of the harmonics, which basically depends on whether the system is written in amplitude-velocity or amplitude-flux form.

For non-constant bathymetries, a linear ODE can be derived to compute the shoaling coefficient in the linearized case. We will briefly recall this procedure, and present are compare the shoaling coefficients for the models considered. The nonlinear shoaling properties will instead be investigated numerically in section §4.

3.1 Dispersion properties

The dispersion properties can be investigated by means of a Fourier analysis on a horizontal bottom. Although the derivation of the equations has been based on the assumption of $\sigma^2 \ll 1$ and $\varepsilon = \mathcal{O}(\sigma^2)$, here we work making the hypothesis of $\varepsilon \ll 1$ and arbitrary σ^2. The procedure follows closely the work of Madsen and Schaffer [14]. Taking the non-dimensional form of the models, we introduce a solution of the form:

$$\tilde{\eta} = a_1 \cos(\xi) + \varepsilon a_2 \cos(2\xi); \qquad \tilde{u} = u_1 \cos(\xi) + \varepsilon u_2 \cos(2\xi) \tag{29}$$

with $\xi = \tilde{\omega}\tilde{t} - \tilde{k}\tilde{x}$ and being $\tilde{\omega}$ the non-dimensional angular frequency and $\tilde{k}$ the corresponding non-dimensional wave number:

$$\tilde{\omega} = \frac{L}{\sqrt{g d_0}}\omega; \quad \tilde{k} = Lk$$

We give some details for the derivation for Peregrine's model, the analysis of the other models is similar with small variations discussed in a final remark.

First-order solution. The linear dispersion properties of the models emerge looking at the first-order solution. Substituting (29) in system (5), for instance, and collecting terms of $\mathcal{O}(1)$ leads to the system :

$$\begin{cases} -\tilde{\omega}a_1 + \tilde{k}\tilde{d}u_1 = 0 \\ -\tilde{\omega}u_1 + \tilde{k}a_1 + \sigma^2\tilde{\omega}\dfrac{\tilde{k}^2\tilde{d}^2}{3}u_1 = 0 \end{cases}, \tag{30}$$

which can be easily solved, giving

$$\begin{cases} u_1 = \dfrac{\tilde{\omega}}{\tilde{k}\tilde{d}}a_1 \\ \dfrac{\tilde{\omega}^2}{\tilde{k}^2\tilde{d}} = \dfrac{1}{1+\frac{\tilde{\phi}^2}{3}} \end{cases}, \tag{31}$$

with $\tilde{\phi} = \sigma\tilde{k}\tilde{d}$. The second equation of (31) represents the non-dimensional phase velocity $\tilde{c}$ of the Peregrine model which, expressed in terms of dimensional variables becomes :

$$c^2 = \frac{\omega^2}{k^2} = \frac{gd}{1+\frac{\phi^2}{3}}, \tag{32}$$

with $\phi = \sigma k d$. This represents the rate at which the phase of the wave propagates in space (so the velocity at which every frequency of the wave propagates) ; in this sense it represents the linear dispersion relation for the Peregrine model. The reference to which this value must be compared is the linear dispersion relation of Stokes :

$$\left(c^2\right)^{Stokes} = gd\frac{tanh(\phi)}{\phi} \tag{33}$$

Figure 2 summarizes the linear dispersion characteristics of the models considered here. The figure reports the ratio c/c^{Stokes} for all the models considered. As anticipated, the eight

systems of PDEs introduced reduce in the linearized case and for constant bathymetry to only three families of linear dispersion relations, which explains the presence of only four curves in the figure, including the exact solution.

The linear dispersion relations depend on the choice of the values of the tuning parameters α_B, β and θ. For all the models one can match the Padé approximation of the dispersion relations of the Stokes wave theory. This can be quickly shown to lead to the following relations between the parameters of the different enhanced models [13] :

$$\beta = \alpha_B/3; \qquad \theta = \sqrt{\frac{1-2\alpha_B}{3}} - 1 \tag{34}$$

The comparison can thus be done by using α_B as the only tuning parameter. As shown on figure 2, in fact, the Beji-Nadaoka and Madsen-Sørensen curves are superimposed, and correspond to the classical choice of $\alpha_B = 0.2$ [4, 15]. Setting $\alpha_B = 0.17$, yields the optimum value for model of Nwogu [16].

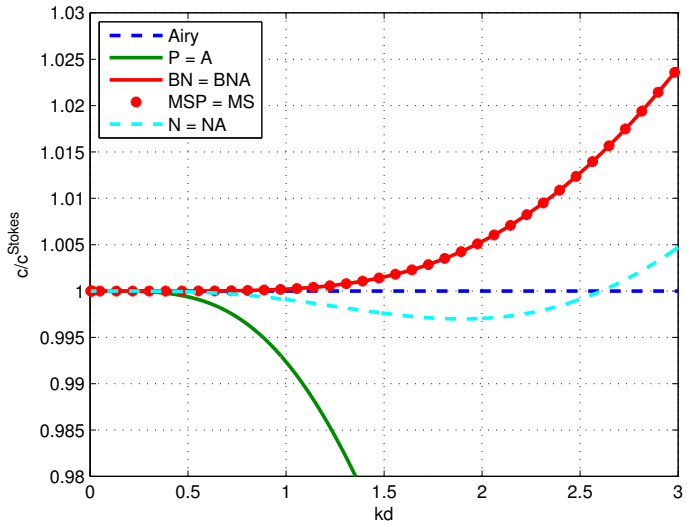

Figure 2: Phase velocity ratio for all the models : P stands for Peregrine (eq. (3)), A for Abbott (eq. (8)), BN and BNA for Beji-Nadaoka and Beji-Nadaoka-Abbott (eq.s (11) and (12) resp.), MS and MSP for Madsen-Sørensen and Madsen-Sørensen-Peregrine (eq.s (14) and (17) resp.), and N and NA for Nwogu and Nwogu-Abbott (eq.s (22) and (26) resp.).

Second-order solution. After (29) has been introduced into the system (5), and collecting terms of $\mathscr{O}(\varepsilon)$, one obtains :

$$\begin{cases} -2\tilde{\omega}a_2 + 2\tilde{k}\tilde{d}u_2 + \tilde{k}a_1u_1 = 0 \\ -2\tilde{\omega}u_2 + 2\tilde{k}a_2 + \dfrac{\tilde{k}}{2}u_1^2 - \dfrac{8}{3}\sigma^2\tilde{k}^2\tilde{\omega}u_2 = 0 \end{cases}. \tag{35}$$

Using the first equation of system (31), we can obtain:

$$\begin{pmatrix} \tilde{m}_{11} & \tilde{m}_{12} \\ \tilde{m}_{21} & \tilde{m}_{22} \end{pmatrix} \begin{pmatrix} a_2 \\ u_2 \end{pmatrix} = \frac{a_1^2}{\tilde{d}} \begin{pmatrix} \tilde{F}_1 \\ \tilde{F}_2 \end{pmatrix} \tag{36}$$

with:

$$\tilde{m}_{11} = 2\tilde{\omega}; \quad \tilde{m}_{12} = -2\tilde{k}\tilde{d}; \quad \tilde{m}_{21} = -2\tilde{k}; \quad \tilde{m}_{22} = 2\tilde{\omega}(1 + 4/3\tilde{\phi});$$

$$\tilde{F}_1 = \tilde{\omega}; \quad \tilde{F}_2 = \frac{\tilde{\omega}^2}{2\tilde{d}\tilde{k}}$$

Solving the linear system, using the dispersion relation to simplify $\tilde{\omega}$, and passing to dimensional variables, leads to the expression :

$$a_2 = \frac{3}{4}\frac{a_1^2}{d}\frac{1}{\phi^2}\left(1 + \frac{8}{9}\phi^2\right) \tag{37}$$

with $\phi = kd$. this value can be compared to the one found for the Stokes theory [14] :

$$a_2^{Stokes} = \frac{1}{4}\left(\frac{a_1^2}{d}\right)\phi\coth(\phi)(3\coth^2(\phi) - 1) \tag{38}$$

Remark 3.1. *In adapting this procedure to the several BT models of section 2, a particular attention must be paid for the A, MS and NA systems. For these models, the relevant ansatz is* $\tilde{q} = q_1\cos(\xi) + \varepsilon q_2\cos(2\xi)$. *Subsequently,*

$$\varepsilon\frac{\tilde{q}^2}{\tilde{d} + \varepsilon\tilde{\eta}} = \varepsilon\frac{\tilde{q}^2}{\tilde{d}} + \mathcal{O}(\varepsilon^2).$$

which can be used to show

$$\varepsilon\left(\frac{\tilde{q}^2}{\tilde{d} + \varepsilon\tilde{\eta}}\right)_{\tilde{x}} = \varepsilon 2\tilde{k}\frac{q_1^2}{\tilde{d}}\sin(\xi)\cos(\xi) + \mathcal{O}(\varepsilon^2).$$

The analysis of the first and second harmonics can then be performed assembling the proper order linear systems as shown for the Peregrine equations.

The results obtained for the different models are compared on figure 3 in terms of the ratio a_2/a_2^{Stokes}. The first obvious remark is that the second harmonic, taking into account the nonlinear behavior of the PDEs, reveals six different families of models. This is expected since, as already remarked, for flat bathymetry the MS and BNA models and the MSP and BN coincide.

The most striking result, however, is that only two different trends are observed depending uniquely on whether the model is in amplitude-velocity or amplitude-flux form. In particular, all the models in amplitude-flux form underestimate, the error monotonically increasing as the reduced wavenumber increases. On the contrary, all the models in amplitude-velocity form give a non-monotone trend, with an initial overestimation of the amplitude, and a peak close to $kd = 1$ for the enhanced models. Also, the error obtained with this class of models is smaller, the ration being closer to one.

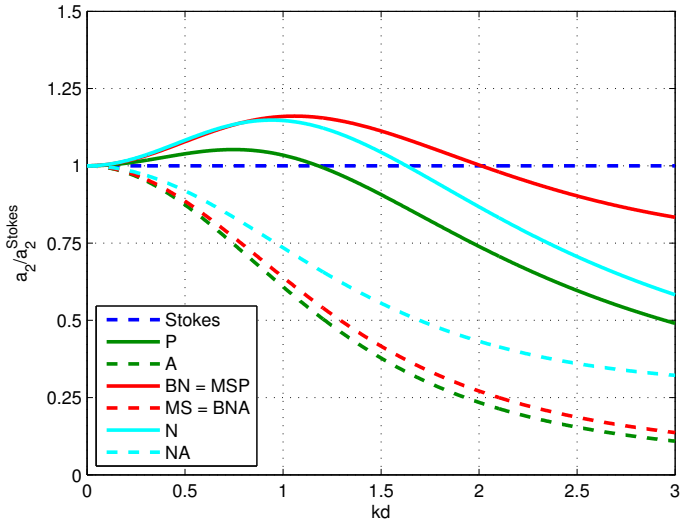

Figure 3: Ratio of the second harmonic a_2/a_2^{Stokes} for the models considered. Continuous line : amplitude-velocity models. Dashed lines : amplitude-velocity models. Refer to figure 2 for the legend.

3.2 Shoaling properties

To characterize the representation of wave shoaling in the linear case, one introduces the shoaling coefficient s which relates the rate of change in wave amplitude to the rate of change in depth :

$$\frac{A_x}{A} = -s\frac{d_x}{d} \tag{39}$$

The procedure to compute the explicit expressions for the coefficient s is described in many papers and textbooks, see e.g. [8, 4, 15, 10, 13]. To be able to actually compare the results of the analysis to the results obtained by numerically solving the models, there is a small catch, not often underlined in literature. To explain this, consider the main ansatz of the linear shoaling analysis, which is the assumption of a "moving shoaling" signal

$$\eta = A(x)\sin(k(x)x - \omega(x)t)\,.$$

This is injected into the model equations to derive ODEs for all the quantities involved, and allows to derive an analytical expression of the type $s = (d, k)$. We refer to the references given for the details of this procedure. We underline, however, that for a given variation (usually linear) of the bathymetry, the local wavenumber $k(x)$ must also be obtained by solving an ODE of the type

$$\frac{k_x}{k} = -\gamma\frac{d_x}{d} \tag{40}$$

where $d(x)$ is defined by the test set and the expression for γ can be found in literature ([15, 4, 13] etc). The values of the shoaling parameter, can be thus represented in two ways.

The one which is most classically reported is $s_0 = s(d(x), k_0)$, representing its variation w.r.t. $k_0 d$, where k_0 is the wave number of the incoming wave. This leads to the classical result reported on the left on figure 4 for the models considered here[1]. However, the variation shown in the picture is not the actual one obtained in practice. To obtain this variation, one must integrate (40) to obtain $k(x)$, and use it to modify $s(d(x), k(x))$ when integrating (39) to compute the actual wave amplitudes. The shoaling coefficient can then still be plotted against $k_0 d$, by computing for a given x the corresponding values of $k_0 d(x)$, and the local value of $s(d(x), k(x)) = -A_x(x)d(x)/(A(x)d_x(x))$. This results in the right picture on figure 4, similar to the one reported without any explaination in [15]. Note that only when including the variation of the wavenumber in the integration of 39 the correct amplitudes are obtained.

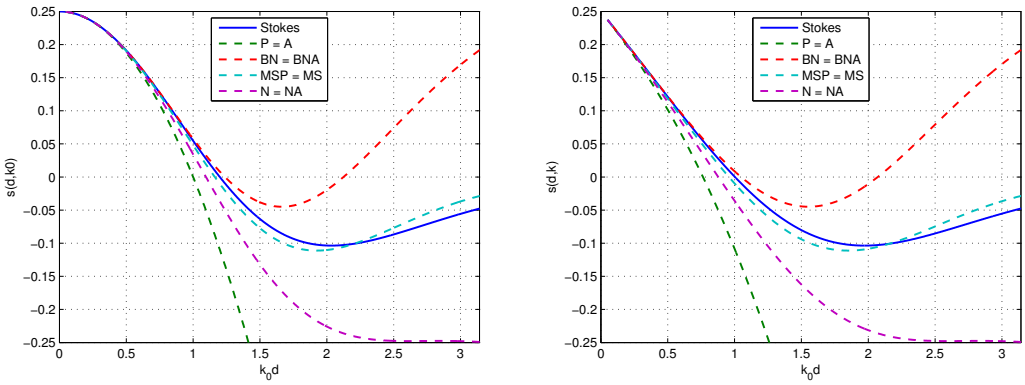

Figure 4: Linear shoaling: representation of the linear shoaling coefficient s of the several BT models defined by (39). On the left is sketched $s(h(x), k_0)$, thus computing the values of s using the initial wavenumber of the signal k_0. On the right, instead, the variation of k along the domain is considered in the computation of the shoaling coefficient, thus: $s(h(x), k(x))$.

For completeness we discuss the comparison of the s coefficient for the models considered in this paper. Figure 4 shows classical results : the Peregrine (and Abbott) model shows a large error already for small wavenumbers with considerable low values of s ; the model of Nwogu gives a better approximation yet still underestimating the wave amplitude already for moderate wavenumbers ; the model of Madsen and Sørensen gives the best approximation among the models considered here ; the model of Beji and Nadaoka overestimates the wave amplitudes, with errors similar to those of the model of Nwogu.

4 Numerical experiments

4.1 Numerical discretization and implementation

The main aim of the numerical tests is to further study the properties of the models in the nonlinear range. In particular, we want to characterize the shoaling characteristics in regions close to breaking conditions. To achieve this, one should require the numerics to be well

[1]The optimal values of the free parameters give in section §3.1 are used for the plot

validated, and the results to be as much as possible independent on the numerical methods. For this reason, we have proceeded as follows. Two different numerical discretizations have been used for each test, which has been performed on several meshes, to guarantee as much as possible scheme and grid independence. In particular, we have used both a finite difference scheme, and a finite element one. The finite difference scheme, is based on the approach proposed by Wei and Kirby, which discretizes the shallow water terms of the equations using the fourth-order finite difference formula, while the dispersive terms to second order accuracy [24]. The finite element method used is instead a P1 continuous finite element discretization based on a standard Galerkin finite element solution of the elliptic sub-problems which define the auxiliary variables $P(\cdot)$, $Q(\cdot)$, $\check{Q}(\cdot)$, $\bar{Q}(\cdot)$, etc, plus a standard Galerkin projection for the first order time dependent PDEs of the several models taken into account: (3), (8), (11), (12), (14), (17), (22), (26). This procedure, introduced in [23] to discretize the model of Nwogu, has been also recently used in [19] to solve the MS equations, and shown both analytically and numerically to have accuracy close to a fourth order finite difference scheme, and to that of the scheme of [24]. In all the tests the two different space discretizations have led to virtually indistinguishable results. In the following we will not show this comparison, but only report the main findings.

We will discuss two type of tests : initial verification benchmarks, in which the results are compared to analytical solutions for both flat and variable bathymetry ; physical experiments, in which we have investigated the behavior of the models in conditions close to wave breaking.

4.2 Initial validation

We will discuss two verification tests : the propagation of solitary waves over a flat bathymetry, and a linear shoaling test. These allow to verify our implementation of the models. Additionally, the linear shoaling tests allow to show that in the linear regime all the numerical models actually do recover the behavior predicted by the linear shoaling analysis.

4.2.1 Soliton propagation

In this section we consider the approximation of exact solitary wave solutions of the models presented. Quite often in literature approximate solitary waves are used. Our purpose here is to be able to quantitatively certify our implementation. For this reason we have chosen to use semi-analytical solutions. These solutions are obtained by generalizing the technique described in [17], and applied to the MS system of equations in [19], consisting in deriving a nonlinear ODE describing the shape of the solitary wave w.r.t the reduced parameter $\xi = x - C\,t$, with C a propagation speed which is also an output of the analysis, hence model dependent.

Details on the computation of these solutions, and the physical and mathematical conditions for their existence are given in [5]. The resulting solitary wave shapes are reported in figure 5 for a wave of amplitude $A/d_0 = 0.2$. Surprisingly, two families of solitaries seem to emerge, models in amplitude-velocity form giving steeper and more peaky profile.

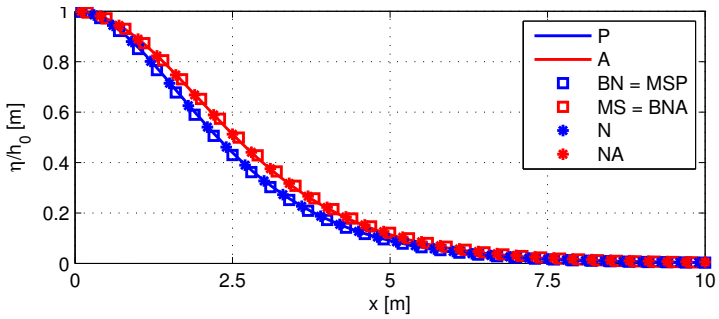

Figure 5: Semi-analytical exact solitary waves for the Boussines models of the paper.

To verify our implementation of the models , we have performed a grid convergence analysis on the solitary wave of figure 5, characterized by and amplitude $A/d_0 = 0.2$, with $d_0 = 1\,[m]$. The numerical results have been compared to the analytical (initial) profile after the wave has travelled for a length of $100\,[m]$. The meshes used for the tets contain 1000, 2000, 4000 and 8000 equally spaced cells. The results are summarized in terms of convergence of the L^2 error on the save amplitude in figure 6. The slopes obtained for the error show a convergence with third order of accuracy for all the models with the exception of the Nwogu-Abbott one (26). The accuracy obtained for the other models is similar to the one shown for the same schemes in [19] in the case of the Madsen and Sørensen equations, and confirms a proper implementation.

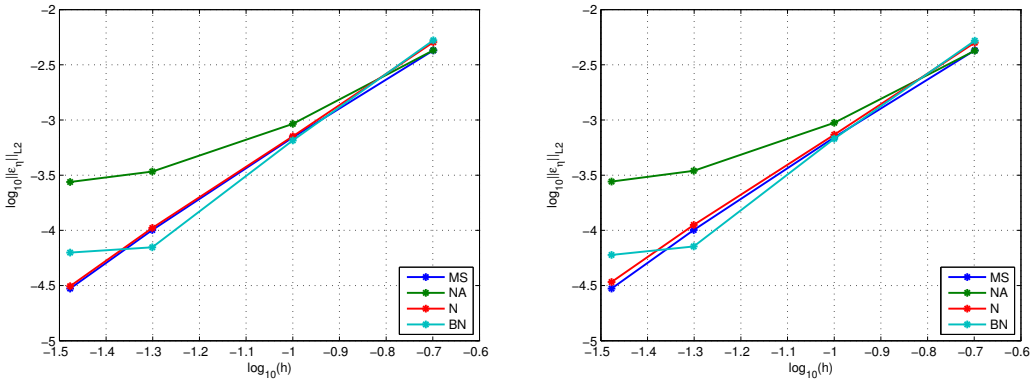

Figure 6: Grid convergence results for the Galerkin finite element (left) and Wei and Kirby finite difference (right) scheme.

The lack of convergence observed for the Nwogu-Abbott equations was at first quite surprising since the solution looks excellent at a simple visual inspection as shown on the left picture on figure 7. A closer inspection has revealed that actually a relatively large error at the foot of the solitary is produced by the semi-analytical technique of [5], especially when compared to the accurate and smooth profiles obtained for the other models. This error seems to be related to the nature of the nonlinear ODEs solved in [5] to compute the exact solitary wave for the Nwogu-Abbott model, and is currently still an unsolved issue.

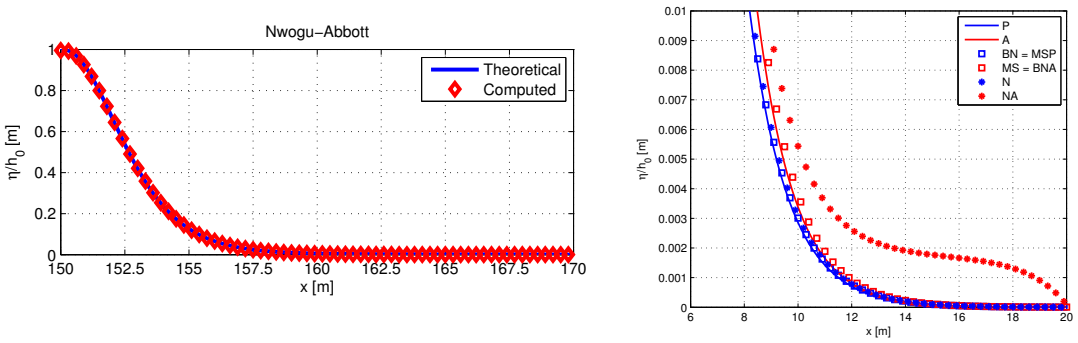

Figure 7: Solitary wave propagation. Left : comparison between numerical and analytical solution for the NA model. Right : error at the foot of the semi-analytical wave for the NA model

4.2.2 Linear shoaling test

To further verify our implementation we have performed the shoaling test proposed by Madsen and Sørensen in [15]. A periodic signal of amplitude $a = 0.05$ m and period $T = 4$ s propagates over an initial constant water depth of $h_0 = 13$ m. The periodic signal has been generated using a source method discussed in [19, 24]. The source of the periodic wave have been set at $x_0 = 100$ m of the domain $[0, 850]$ m. The bottom is flat for the first 50 m from the position of the periodic wave generator, it has a constant up-slope of $1 : 50$ from $x = 150$ m to $x = 800$ m and it then returns flat until the end of the domain. In this way the local values of the parameter $\varepsilon = a_0/h$, which represents the effects of nonlinearity, vary between the values 0.0038 and 0.25, attesting we are working in the linear regime and the nonlinear effects can be actually considered negligible. Two 60 m wide absorbing sponge layers have been used at the two boundaries of the domain restricting the region of study of the shoaling to $x = 790$, but avoiding undesirable reflections due to the upper bottom shape discontinuity. The finest mesh used has a uniform grid size of $\Delta X = 0.333$.

For this test case a theoretical envelope of the signal amplitude can be obtained from the linear shoaling analysis by integrating (39). This curve is used as a reference to compare and validate the numerical results. For this particular case, the theoretical envelopes of the models are sketched on the left picture on figure 8, while the right picture shows the typical wave profiles obtained[2].

[2]Result of the Madsen and Sørensen model.

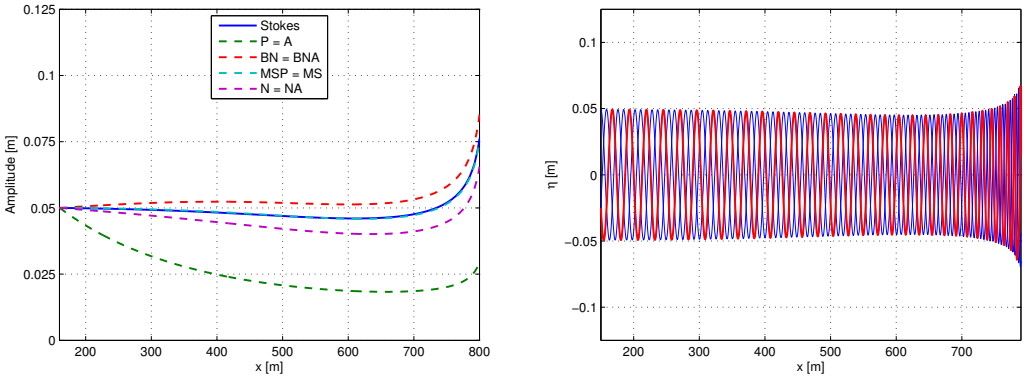

Figure 8: Linear shoaling. Left : theoretical envelope of the maximum wave amplitude. Right: line plots of the surface elevation computed using the MS model.

The comparison of the envelopes obtained by numerically solving the models with the theoretical ones is summarized on figure 9. We can observe that the theoretical results are very well-reproduced by all the models and that, as expected, the MS and MSP models produce almost superimposed results, as well as the BN and BNA models, and the N and NA ones. Very close to the end of the slope, nonlinear effects start begin non-negligible, and we can clearly see a difference appearing between the linear theory and the numerical solution of the nonlinear equations.

The curves corresponding to the P and A models are not present in figure 9 due to the fact that for such low amplitude waves we where unable to obtain a stable periodic signal by the internal wave generator strategy, at least not in the form described in [19] and implemented here.

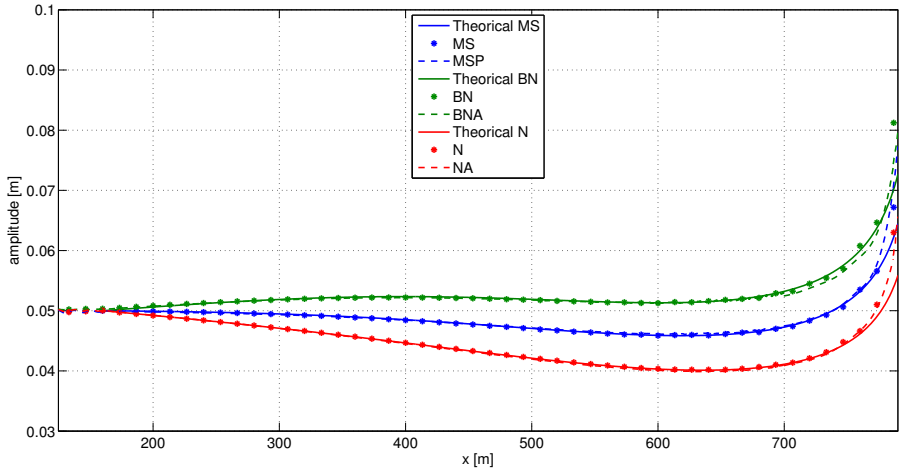

Figure 9: Linear shoaling: maximum elevation

4.3 Physical experiments

In this section finally we investigate the nonlinear properties of the models. We consider two experiments. The first is the nonlinear shoaling tests of [9]. The second involves the propagation of monochromatic waves over a submerged bar in two configurations : a non-breaking, and a breaking one. For the second configuration no breaking model is included. However, the results will allow to study and compare the shape of the wave obtained with the different models in a more complex flow.

4.3.1 Nonlinear shoaling test

This test allows to study the wave shoaling characteristics obtained with the models considered in conditions close to wave breaking. The test has been initially proposed by Grilli et al. in [9], and it consists of a solitary wave of amplitude $A/d_0 = 0.2$ m propagating on a water depth $d_0 = 0.44$ m, and shoaling onto a constant slope of $1 : 35$. Note that in this test the local values of the nonlinearity parameter are roughly $\varepsilon = a_0/h \in [0.2; 2.2]$, which is clearly in the nonlinear range $\varepsilon \geq 1$. A representation of this test is given below in figure 10.

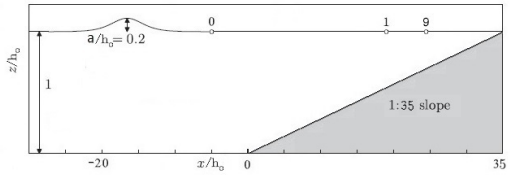

Figure 10: Shoaling of a solitary wave; computational configuration and gauges position.

The numerical results obtained with the models studied in the paper are compared to the data of the laboratory experiments of [9]. The data available consist in the values of the

free-surface elevations measured in 10 gauges positioned at stations from 0 to 9 (figure 10), with gauge 0 positioned just before the toe of the slope and gauge 9 located close to the wave breaking point. We refer to [9] for the precise description of the setup.

In our test, gauge 0 is used to calibrate the phase of the solutions obtained, the semi-anaytical solitary waves traveling at a celerity depending on the form of the model. The resulting shoaling wave profiles are compared to the experiments in figures 11 and 12, while the spatial evolution of the peak height is compared to the experiments in figure 13.

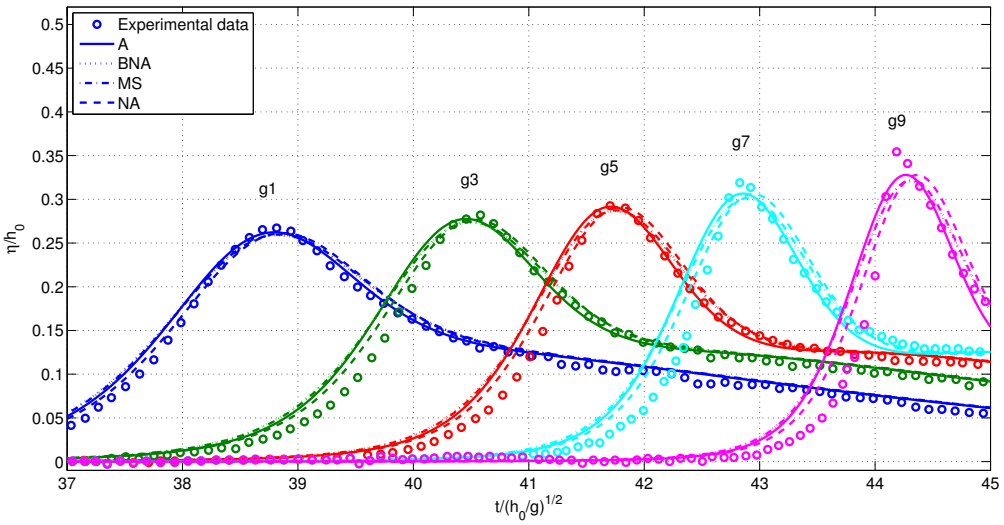

Figure 11: Nonlinear shoaling. Comparison between computed wave heights at gauges 1, 3, 5, 7 and 9 and data of [9] ; models in amplitude-flux form.

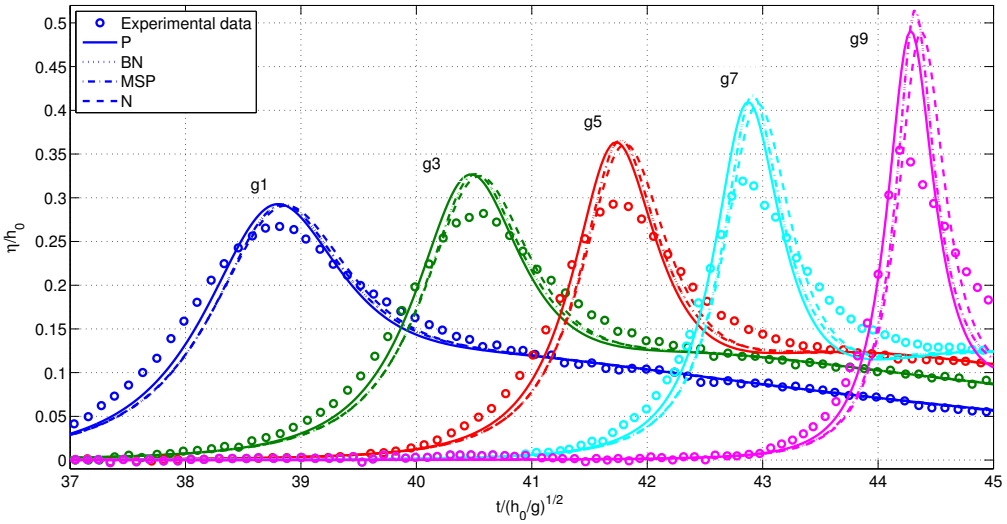

Figure 12: Nonlinear shoaling. Comparison between computed wave heights at gauges 1, 3, 5, 7 and 9 and data of [9] ; models in amplitude-velocity form.

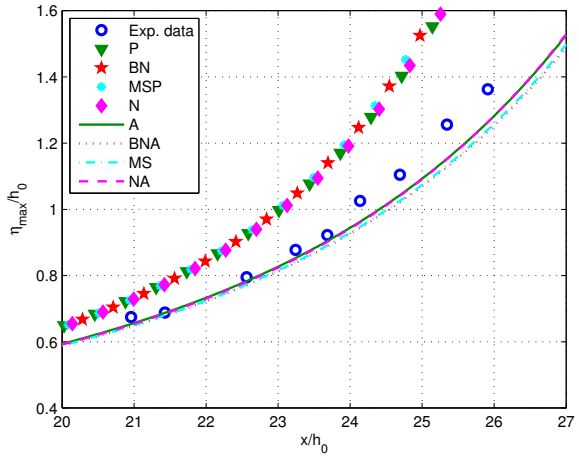

Figure 13: Nonlinear shoaling. Comparison between computed wave peak evolution and data from [9].

The results show two distinct behaviors. All the models in amplitude-velocity form provide waves with considerably higher peaks and fronts with larger slope compared to the data, while all the models in amplitude-flux form give shorter waves with smaller slopes. This independently on the quality of the linearized system.

This result is extremely important if one is to use these models in conjunction with a breaking detection plus dissipation mechanism. In particular, whether based on the slope of the front, on wave curvature, or on wave height, two distinct parametrizations of the detection criterion are necessary for these two family of models. In particular, looking at gauge 9, which

is roughly where wave breaking should be detectable, we can see that while amplitude-velocity models have front slopes and wave heights larger than those of the data, velocity-flux models give lower amplitudes and, more importantly, much smaller front slopes. For criteria based on the shape of the profiles, such as those discussed e.g. in [21, 11], this might mean that for a given parametrization of the constants involved in the breaking criterion, amplitude-velocity models might give an early breaking, while amplitude-flux models will most likely give a late breaking, or not break at all. We remark once more, that this result is independent on the quality of the model in terms of linear phase accuracy, the models of Peregrine and Abbott giving results considerably close to their enhanced versions.

4.3.2 Periodic wave propagation over a submerged bar

The last test is meant to verify the behavior of the models in a more complex situation. We consider the classical tests of monochromatic waves propagating on a submerged bar, for which extensive experimental data exist [3]. The geometry of the tests considered is sketched on figure 14. Monochromatic waves are generated and propagate on a depth of $d_0 = 0.4$ m before reaching the submerged bar. The periodic wave shoal over the 1:20 front slope, developing higher harmonics which are then released from the carrier frequency on the 1:10 slope of the lee side of the obstacle. We consider two configurations. Case (a) : wave amplitude $A/d_0 = 0.025$ and period $T = 2.02$s. Case (b) : wave amplitude $A/d_0 = 0.0675$ and period $T = 2.525$s. The first case is often used to validate dispersive wave propagation models. In the second case, considerably nonlinear conditions are obtained toward the end of the slope, where breaking is known to occur.

The periodic wave is generated by means of a periodic wave generator placed at $x = 10$ m of the domain $[0, 35]$ m and two sponge layers with 3 m of thickness are used at the two boundaries of the domain in order to absorb any wave reaching the boundaries. In both the cases, the finest grid used has a grid size of $\Delta X = 0.04$ m. The numerical results are compared with the data of Beji and Battjes [3]. In particular, in both cases the first gauge is used to phase calibrate the signal of the simulations with the experiments, while the other probes are then used to compare and validate the models. For further details on the tests, and for the exact location of the gauges the interested reader can consult [3, 8, 11].

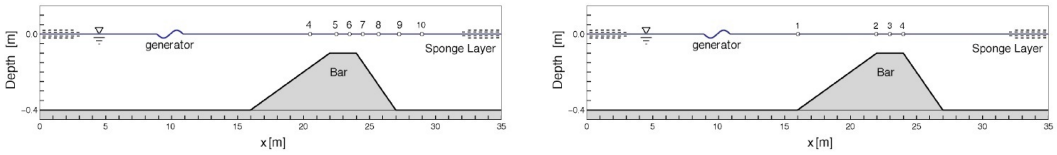

Figure 14: Periodic wave propagation over a submerged bar: sketch of the computational configuration and of the gauges position; case (a) on the left, case (b) on the right.

Case (a). In this case, the wave signal has been phase calibrated w.r.t. the experimental data at gauge 4. The result is shown on figure 15. In figures 16, 17, 18 and 19, we show the comparison between computed and experimental signals. In all the figures, the continuous

lines are used for models in amplitude-flux form, and dashed lines for models in amplitude-velocity form. For brevity, we only consider gauge 5, position on the plateau, and gauge 10, which is placed after the obstacle.

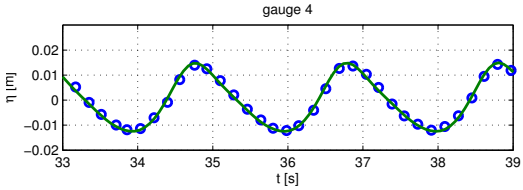

Figure 15: Propagation over a submerged bar, case (a); data in gauge 4 are used for the signal syncronization.

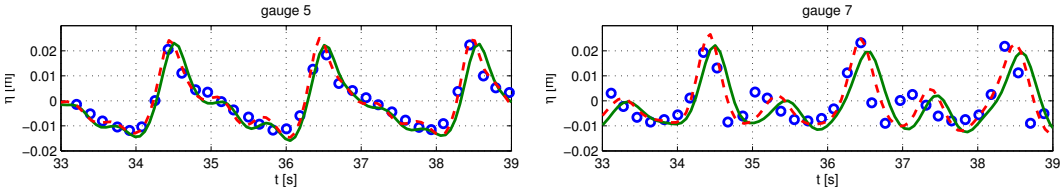

Figure 16: Propagation over a submerged bar, case (a); data in gauge 5 (left) and gauge 10 (right): experimental data [3] (o), A model (—), P model (- -).

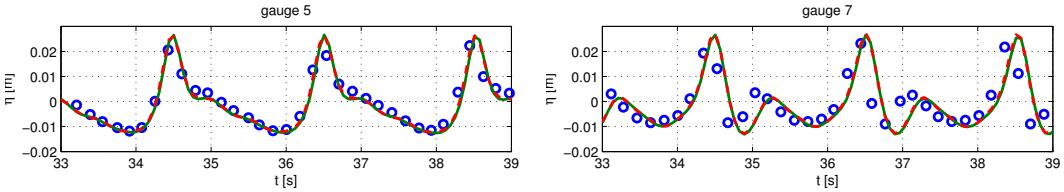

Figure 17: Propagation over a submerged bar, case (a); data in gauge 5 (left) and gauge 10 (right): experimental data [3] (o), BNA model (—), BN model (- -).

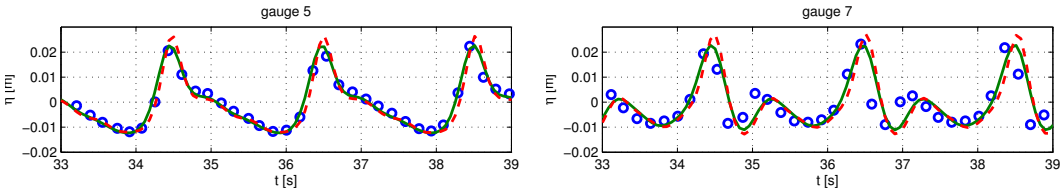

Figure 18: Propagation over a submerged bar, case (a); data in gauge 5 (left) and gauge 10 (right): experimental data [3] (o), MS model (—), MSP model (- -).

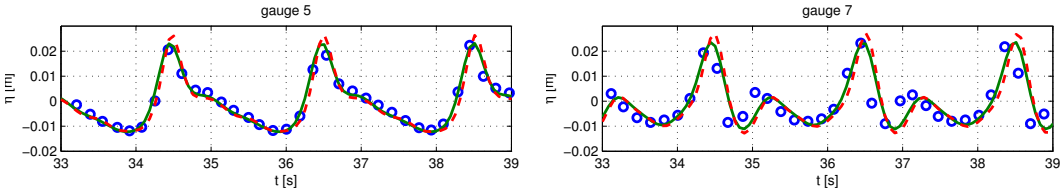

Figure 19: Propagation over a submerged bar, case (a); data in gauge 5 (left) and gauge 10 (right): experimental data [3] (o), NA model (—), N model (- -).

The following remarks can be made. On the plateau, after shoaling has occurred, models in amplitude-velocity form give waves which have slightly higher peaks and steeper slopes, however the differences are small (roughly 5%d or below). The main remark that can be perhaps made is that the models of Peregrine and Abbott seem to have a larger phase advance in gauge 7 when compared to the other models. This is confirmed by the data in section 10, reported for completeness in figure 20, where the models of Paregrine and Abbott are compared with the respective Nwogu enhanced variant, giving results very similar to those of the other models. The picture shows that clearly for this case having a good approximation of the linear dispersion relations is more important than the form of the models.

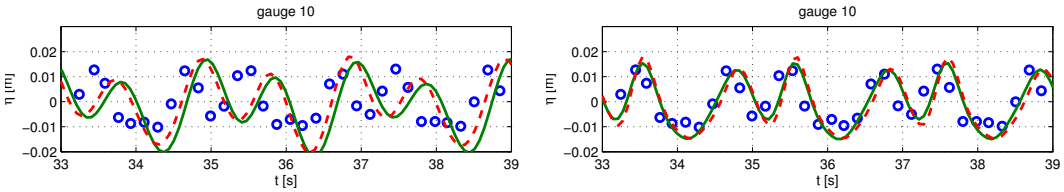

Figure 20: Propagation over a submerged bar, case (a); data in gauge 10 for the models of Peregrine and Abbott (left), and for the enahnced variants of Nwogu ad Nwogu-Abbott (right). Experimental data [3] (o). Left figure : A model (—), P model (- -). Right figure : NA model (—), N model (- -).

Case (b). In this case, wave breaking is expected to occur around gauge 2, at the end of the slope. As already remarked, no breaking criteria are included in our results so that the nonlinear behavior of the Boussinesq models is observed. For this case, the numerical results are phase calibrated w.r.t. experimental data measured at gauge 1, as shown in figure 21.

We then compare the computed wave heights with the data in gauge 2, at the end of the slope, and gauge 4, at the end of the plateau. The results are reported on figures 22, 23, 24 and 25. As before, in all the figures continuous lines are used for models in amplitude-flux form, and dashed lines for models in amplitude-velocity form.

From the figures we can see that already in gauge 2 there is a substantial difference in the height of the peak, with models in amplitude-velocity form giving peaks with taller wave heights, with differences of more than 20%d, and consequently, steeper wave fronts. This difference is even more visible in gauge 4, where the difference gous up to more that 35%d. models in amplitude-flux form clearly give gentler slopes, and shorter waves. As for the nonlinear shoaling test section §4.3.1, the results are practically independent on the linear characteristics of the systems, and only depend on the fact the the model is in amplitude-velocity, or amplitude-flux form.

Once more, from the point of view of wave breaking detection, we see that the same criterion cannot be applied to models of the two families, or anyways not with the same parametrization.

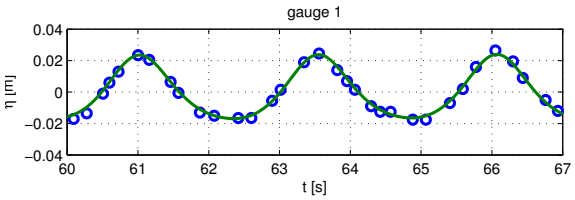

Figure 21: Propagation over a submerged bar, case (b); data in gauge 1 are used for the signal syncronization.

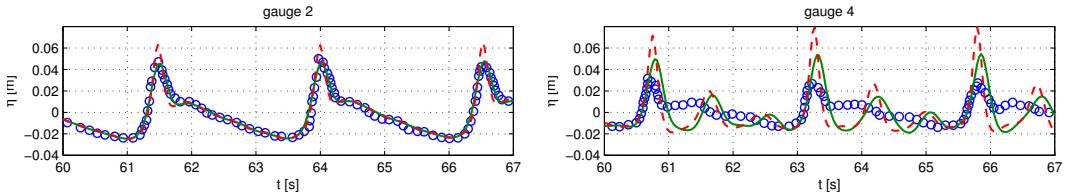

Figure 22: Propagation over a submerged bar, case (b); data in gauge 2 (left) and gauge 4 (right): experimental data [3] (o), A model (—), P model (- -).

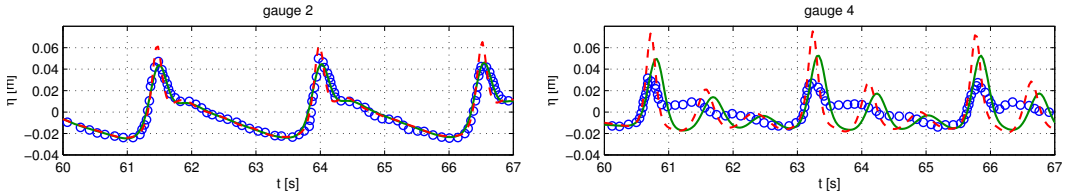

Figure 23: Propagation over a submerged bar, case (b); data in gauge 2 (left) and gauge 4 (right): experimental data [3] (o), BNA model (—), BN model (- -).

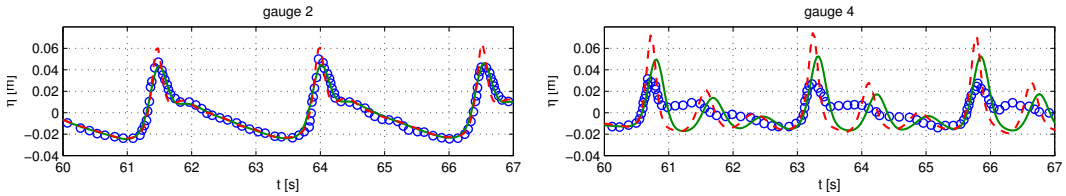

Figure 24: Propagation over a submerged bar, case (b); data in gauge 2 (left) and gauge 4 (right): experimental data [3] (o), MS model (—), MSP model (- -).

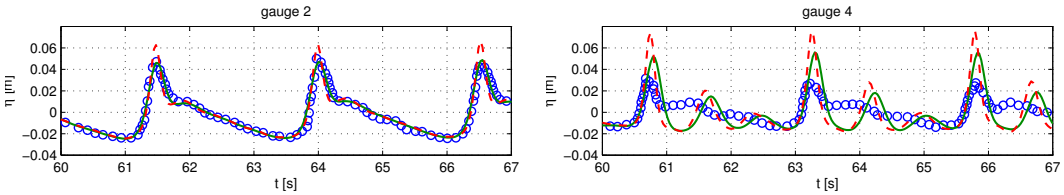

Figure 25: Propagation over a submerged bar, case (b); data in gauge 2 (left) and gauge 4 (right): experimental data [3] (o), NA model (—), N model (- -).

5 Conclusions and perspectives

In this paper we have considered the impact of the form of weakly nonlinear Boussinesq models on their behavior in situations in which nonlinearity is not negligible. We have recalled how, within the same asymptotic truncation, a given linearized form, hence a give dispersion relation and shoaling coefficient, allow two derive two sets of PDEs : one, referred to as amplitude-velocity form, in which dispersive terms contain differential operators applied to the velocity ; the other, referred to as amplitude-flux form, in which these operators are applied to the flux. We have give four examples of these couples, including a new formulation of the model of Nwogu in terms of the flux.

The analytical and numerical study of these models has shown that : as soon as nonlinear effects start being relevant, the main factor influencing the behavior of the model is its amplitude-velocity or amplitude-flux form, enhanced models giving the same results as Peregrine's or Abbott's equations. This fact has been demonstrated analytically by the study of the propagation of higher harmonics, following [14], and numerically on tests involving shoaling in genuinely nonlinear regimes. So, while in the linear case we have as many families of models as the number of linear dispersion relations times the linear shoaling coefficient, in the nonlinear case, only two type of behavior are observed.

This work has important consequences on the way in which wave breaking conditions are applied to these models, as well as on the way in which wave breaking dissipation is included. Clearly, breaking criteria should not be the same for the two family of models, and perhaps even the amount of dissipation in breaking regions necessary in the two cases should be different.

Future development of this work will definitely involve the study of the coupling of the models considered in this paper with physical breaking criteria as those used in e.g. [2, 11, 22, 21] and references therein. Other future developments will involve the study of deep water models, as well as the one-to-one comparison of different forms of weakly-nonlinear with fully nonlinear models coupled with breaking detection and dissipation mechanisms.

References

[1] M.B. Abbott, H.M. Petersen and O. Skovgaard: Computations of short waves in shallow water. Coast.Eng., (1978).

[2] P. Bacigaluppi, M. Ricchiuto and P. Bonneton: A 1D Stabilized Finite Element Model for Non-hydrostatic Wave Breaking and Run-up. Finite Volumes for Complex Applications VII-Elliptic, Parabolic and Hyperbolic Problems, Springer Proceedings in Mathematics & Statistics, (2014) vol. 78, pp. 779–790, isbn 978-3-319-05590-9

[3] S. Beji and J.A. Battjes: Numerical simulations of nonlinear-wave propagation over a bar. Coast.Eng., (1994) vol 23,

[4] S. Beji and K. Nadaoka: A formal derivation and numerical modeling of the improved Boussinesq equations for varying depth. Ocean Eng., (1996), vol. 23, pp.1–16

[5] S. Bellec abd M. Colin : On the existence of solitary waves for Boussinesq type equations and a new conservative model. In preparation.

[6] M. Brocchini: A reasoned overview on Boussinesq-type models: the interplay between physics, mathematics and numerics. Proc. Royal Soc. A, 2014

[7] R. Cienfuegos and E. Barthelemy and P. Bonneton: A fourth order compact finite volume scheme for fully nonlinear and weakly dispersive Boussinesq type equations. Parti II: Boundary conditions and validation. Int. J. Numer. Meth. Fluids, (2006), vol 53.

[8] M.W. Dingemans : Water wave propagation over uneven bottoms. Advanced Series Ocean Eng., (1997), World Scientific

[9] S.T. Grilli, R. Subramanya, I.A. Svendsen and J. Veeramony: Shoaling of solitary waves on plane beaches. J.Waterw.Port.C.-ASCE, (1994), vol. 120

[10] M. Kazolea: Mathematical and computational modeling for the generation and propagation of waves in marine and coastal environments. PhD, Technical University of Crete, (2013).

[11] M. Kazolea, A.I. Delis and C. Synolakis: Numerical treatment of wave breaking on unstructured finite volume approximations for extended Boussinesq type equations. J.Comput.Phys.,(2014)

[12] D. Lannes: The water waves problem. Mathematical analysis and asymptotics. Mathematical Surveys and Monographs, (2013), Americal Mathematical Society

[13] C. Lee, Y.S. Cho, S.B. Yoon: A note on linear dispersion and shoaling properties in extended Boussinesq equations. Ocean Eng.,(2003), vol.30, pp.1849–1867

[14] P. A. Madsen and H. A. Schaffer: Higher-Order Boussinesq-Type Equations for Surface Gravity Waves: Derivation and Analysis. Phil. Trans. R. Soc. Lond. A, (1998), vol. 356.

[15] P.A.Madsen, O.R.Sorensen: A new form of the Boussinesq equations with improved dispersion characteristics. Part 2: a slowing varying bathymetry. Coast.Eng., (1992), vol.18, pp.183–204

[16] O. Nwogu: An alternative form of the Boussinesq equations for near-shore wave propagation. J.Waterw.Port.C.-ASCE, (1994), vol. 119, pp. 618–638

[17] J. Orszaghova, A.G.L. Borthwick, P.H. Taylor: From the paddle to the beach - A Boussinesq shallow water numerical wave tank based on Madsen and Sørensen's equations. J.Comput.Phys., (2012), vol. 231, pp. 328–344

[18] D.H. Peregrine: Long waves on a beach. J.Fluid.Mech, (1967), vol. 27

[19] M. Ricchiuto and A.G. Filippini: Residual discretization of enhanced Boussinesq equations for wave propagation over complex bathymetries. J.Comput.Phys., (2014), pp. 306–341

[20] V. Roeber and K.F. Cheung: Boussinesq-type model for energetic breaking waves in fringing reef environments. Coast.Eng., (2012), vol. 70, pp. 1–20

[21] M. Tissier, P. Bonneton, F. Marche, F. Chazel and D. Lannes: A new approach to handle wave breaking in fully nonlinear Boussinesq models, Coast.Eng., (2012), vol. 67

[22] M. Tonelli and M. Petti: Simulation of wave breaking over complex bathymetries by a Boussinesq model. J.Hydraulic Res., (2011), vol.49

[23] M.A. Walkley and M. Berzins: A finite element method for the two-dimensional extended Boussinesq equations. Int.J.Numer.Meth Fluids, (2002), vol. 39

[24] G. Wei and J.T. Kirby: A time-dependent numerical code for extended Boussinesq equations. J.Waterw.Port.C.-ASCE, (1995), vol 120, pp. 251–261